



HAL
open science

Damage mechanisms at room and high temperature in notched specimens of Al6061/AlO particulate composites

Elisabetta Gariboldi, Antonietta Lo Conte

► **To cite this version:**

Elisabetta Gariboldi, Antonietta Lo Conte. Damage mechanisms at room and high temperature in notched specimens of Al6061/AlO particulate composites. *Composites Science and Technology*, 2009, 68 (1), pp.260. 10.1016/j.compscitech.2007.03.014 . hal-00509038

HAL Id: hal-00509038

<https://hal.science/hal-00509038>

Submitted on 10 Aug 2010

HAL is a multi-disciplinary open access archive for the deposit and dissemination of scientific research documents, whether they are published or not. The documents may come from teaching and research institutions in France or abroad, or from public or private research centers.

L'archive ouverte pluridisciplinaire **HAL**, est destinée au dépôt et à la diffusion de documents scientifiques de niveau recherche, publiés ou non, émanant des établissements d'enseignement et de recherche français ou étrangers, des laboratoires publics ou privés.

Accepted Manuscript

Damage mechanisms at room and high temperature in notched specimens of Al6061/Al₂O₃ particulate composites

Elisabetta Gariboldi, Antonietta Lo Conte

PII: S0266-3538(07)00121-2
DOI: [10.1016/j.compscitech.2007.03.014](https://doi.org/10.1016/j.compscitech.2007.03.014)
Reference: CSTE 3632

To appear in: *Composites Science and Technology*

Received Date: 3 August 2006
Revised Date: 6 March 2007
Accepted Date: 13 March 2007

Please cite this article as: Gariboldi, E., Conte, A.L., Damage mechanisms at room and high temperature in notched specimens of Al6061/Al₂O₃ particulate composites, *Composites Science and Technology* (2007), doi: [10.1016/j.compscitech.2007.03.014](https://doi.org/10.1016/j.compscitech.2007.03.014)

This is a PDF file of an unedited manuscript that has been accepted for publication. As a service to our customers we are providing this early version of the manuscript. The manuscript will undergo copyediting, typesetting, and review of the resulting proof before it is published in its final form. Please note that during the production process errors may be discovered which could affect the content, and all legal disclaimers that apply to the journal pertain.



**DAMAGE MECHANISMS AT ROOM AND HIGH TEMPERATURE IN NOTCHED
SPECIMENS OF AL6061/AL₂O₃ PARTICULATE COMPOSITES**

Elisabetta Gariboldi, Antonietta Lo Conte

Dipartimento di Meccanica, Politecnico di Milano

Via la Masa 34, 20156 Milano (Italy)

ABSTRACT

The aim of the present study was the investigation of the effects of macroscopic stress triaxiality on the presence and evolution of damage in particulate MMC. Two Al6061/Al₂O₃/10p and 20p particulate reinforced composites were investigated on smooth and differently notched specimens pulled in tension at 20 and 250°C. Fractographic analyses and microstructural observations were carried out in order to identify and to map damage mechanisms. Particle fracture was the prominent form of material damage at 20°C, while debonding was the main damage mechanism at 250°C. The distribution of the two damage forms within the specimen volume was compared to the results of finite element analyses. At a given level of triaxiality (considered as the hydrostatic to Von Mises stress ratio), particle fracture localized in regions of high maximum principal stress, generally associated to the high hydrostatic stress. It was further observed that matrix/interface debonding concentrated in the same regions, developed on other particles at higher/lower load level depending on test temperature.

KEYWORDS

(A) Metal-matrix composites (MMCs), (B) Mechanical properties, (B) High-temperature properties, (C) Damage mechanics, Triaxiality

INTRODUCTION

The mechanical behaviour of MMC has been extensively investigated during the nineties and at the beginning of the millenium. The mechanical properties of MMC are often related to the anticipated onset of microstructural damage, i.e. the process of initiation and growth of microcracks and microcavities, which was often related to particle/matrix interaction [1-3]. The microstructural heterogeneity of MMC strictly affects the form of damage experienced by the composite which, in turn, is related to the local stress effects at the matrix/particle interface as well as inside the particle and the matrix. Particle cleavage, matrix/particle interface debonding or void formation in the matrix are common forms of crack nucleation phenomena leading to fracture. Debonding is typically observed only in MMCs with relatively weak interface bonding [1]. Matrix composition and temper can also be of influence [1-2, 4-5]. The onset and evolution of damage was investigated on a microscale by means of analytical models or FEM simulations [6-9]. On a macroscale, it is easier to consider the MMC as a homogeneous material whose mechanical behaviour is often related to local degradation effects by means of simple damage parameters, that can be differently defined and evaluated by means of indirect measurement methods. In literature [4-6, 8] the evolution of microstructural damage was in general based on the experimental results from uniaxial tensile stresses and on the assumption that a single form of microstructural damage is active.

In general, commercially available particulate MMCs were not specifically developed for high-temperature applications but rather to enhance the room temperature stiffness and mechanical properties. Studies of their mechanical behaviour at intermediate temperature were performed [10-13] to check if, and to which extent, the appealing room temperature characteristics are maintained when the operating temperatures are raised either as a result of accidental overheating or when extension from room to higher temperature applications are considered. It is known that the improvement of tensile strength of these composites with respect to the corresponding massive alloys is reduced to about one third by increasing the temperature from 20 to about 300°C [10, 11]. The short and long-term mechanical characteristic of Al6061/Al₂O₃/10p and Al6061/Al₂O₃/20p composite at temperatures in the range 20-300°C was already investigated by a coauthor of the present paper [11-12] and their results were consistent to those recently reported in literature [13].

Differences in the tension and creep behaviour of such composites corresponds to different microstructural damage mechanisms. Particle/matrix interface debonding prevailed at the higher temperature (particularly in the low stress range where the long test duration led to overaging of the matrix alloy) while at room and intermediate (150°C) temperatures, particle cleavage was found to be the main damage form. The use of the classical phenomenological Rabotnov-Kachanov creep damage model for uniaxial creep tests [14] was able to discriminate between the evolution of the two damage forms [12]. Further, the use of acoustic emission technique suggested that at 20°C particle fracture developed in the early stages of plastic deformation in uniaxial specimens pulled in tension [15]. Under similar conditions the damage rate was relatively high, particularly for matrices of relatively high strength [5].

When multiaxial stress condition are present, as in many industrial components, the material ductility changes as a result of different damage evolution before fracture. The effect of multiaxial loading condition on damage characteristics at room and high temperature will be the topic of the present paper, where triaxiality induced by specimen geometry will be examined. To the authors' knowledge, the effect of the presence of a multiaxial state of stress was investigated in some literature studies, by comparing the surface and inner regions of cracked toughness test specimen [16]. In other cases specific tests were developed, superimposing hydrostatic compression state on pulled uniaxial tensile specimens [18-19], or performing tensile tests on notched specimens [10-21]. The main aims of these studies were in any case either the definition of fracture toughness properties or the increase of material ductility brought about by the presence of compressive hydrostatic stress typical of some metal forming process. The use of notched specimens allows to obtain different degree of triaxiality (even not homogeneously distributed within the cross section of the specimens) simply performing tensile tests on specimens with different notch geometries. Thus in the present study a set of notched specimens was used to obtain different degree of stress triaxiality (hydrostatic to Von Mises stress ratio) on metal matrix composites in order to investigate the effects of stress multiaxiality on material damage.

MATERIALS AND EXPERIMENTAL TESTS

Two commercially available 6061 Al alloys reinforced with 10 vol.% and 20 vol.% Al_2O_3 particles (hereafter referred as Al6061/ Al_2O_3 /10p and Al6061/ Al_2O_3 /20p, respectively) were studied. They were produced by a molten metal process, supplied as 20 mm diameter extruded bars and were investigated in their T6 temper condition. The investigated composites had a fairly homogeneous distribution of equiaxed blocky shaped particles was noticed in both materials. In addition to the volume of reinforcement phase, the difference between the composites consisted also in their particle size. Al6061/ Al_2O_3 /20p include a fraction of relatively large particles, thus having an almost double average particle size.

Conventional cylindrical bar specimens (hereafter referred as CS specimens) having gauge diameter of 10 mm and gauge length of 50 mm were machined. In addition, specimens with an artificially machined ‘natural neck profile’ (NNP specimens) were prepared. The specimen radius (r) varies along the longitudinal axis (z) according to the following equation [22]:

$$r = a_{\infty} \cdot \left[1 - u \left(\sqrt{1 + \frac{1}{\left(\frac{z}{a_{\infty}}\right)^2 + u^2}} - 1 \right) \right] \quad \text{with} \quad v = \frac{\frac{a}{a_{\infty}} \left(2 - \frac{a}{a_{\infty}} \right)}{2 \left(1 - \frac{a}{a_{\infty}} \right)} \quad (1)$$

Symbols a and a_{∞} in equation (1) are the radius at the neck (4 mm) and the specimen radius at a great distance from the neck (9 mm), respectively. Lastly, two sets of circumferentially notched bars, i.e. round bars containing parallel sided notches, were machined for the present study. In both cases the maximum radius (a_{∞}) was 9 mm. In a first set of samples, referred as 2N specimens, the minimum radius (a) and the notch radius (R) were 4.5 and 2.25 mm, respectively, with notch sharpness a/R equal to 2. In the second set of samples (5N specimens) a and R were 3.35 and 0.67 mm, respectively, resulting in notch sharpness 5. The above geometries allowed to obtain different stress distributions in the region of the notch and different maximum levels of triaxiality. The relatively low stress gradients in their minimum cross sectional area makes relatively easy to relate the local stress condition to microstructural features defined on a sufficiently large volume of

material. For these reasons, sets of notched specimens were used in the past to investigate the effect of triaxiality of different metallic materials and to associate different damage forms alternatively, to the maximum principal, hydrostatic, effective (Von Mises) stress [23, 24]. It should be considered that in these notched specimens triaxiality increases as the elastic stress concentration factor increases, from NNP to 2N and 5N specimens. The above specimens, depicted in Figure 1, were pulled in tension at room temperature and at 250°C (heating time about 20 min, soaking time about 10 min) with pulling rate of 0.01 mm/min. In some cases the tensile test was interrupted before final fracture, just after the maximum load was reached.

After mechanical testing, fractographic observations were carried out. Further, tensile specimens were longitudinally sectioned along their axis and prepared for microstructural analyses. Electropolishing with 30 vol% HNO₃, 70 vol% ethanol using 10V voltage for 45 seconds was used to provide surfaces suitable for an optimal identification of microstructural damage during optical and SEM microscopy analyses. A set of micrographs at 250X was taken for each specimen so that the region of the notch or of the final rupture was entirely covered. The area represented by each micrograph (about to 0.15 mm²) was enough to guarantee material homogeneity in terms of particle number per micrograph, since the average particle number per micrograph was about 220 and 285 in Al6061/Al₂O₃/20p and Al6061/Al₂O₃/10p, respectively. Further, the magnification chosen enabled to identify quite clearly the presence of fractured particles and of interfacial decohesions with the matrix. A preliminary manual check was done, defining for each micrograph the area of interest for image analyses computations (overlapping regions were taken into account only once), separating single particles, and identifying for each damaged particle if damage consisted of matrix/interface debonding or of particle fracture. Multiple interface and the presence of both damage types on a single particle were so rare that taking them into consideration would not have altered significantly the obtained results. An image analysis software was then used to count the number of particles per area and to evaluate, for each micrograph, the fraction of debonded and fractured particles (D_d and D_f , respectively). The results were used to map the their distribution.

RESULTS

The results of tensile tests at both temperatures are summarized in Table I. It should be observed that the moderate ductility of the MMCs prevented a careful measurement of reduction of area and data were not reported here. The uniaxial stress-strain curves of the composites followed and thus were modelled by a Ramberg-Osgood constitutive relationships, with the strain hardening constant and exponent listed in the same table 1. Comparing tensile strength (UTS and 0.2%YS) and final elongation (A), the greater strength and lower ductility of the composite with the higher volume fraction of alumina particles (Al6061/Al₂O₃/20p) is evident. It is clear that, as temperature was increased from 20 to 250°C, the composites significantly reduced their tensile strength and increase final elongation. The results of tensile tests for different material, specimen type and test temperature are presented in Figure 2 in terms of ratio between the maximum net stress and the ultimate tensile stress of the unnotched (CS) specimen of corresponding material/temperature plotted as a function of elastic stress concentration factor. At room temperature Al6061/Al₂O₃/10p displayed notch strengthening behaviour (i.e. maximum net stress increased with respect to that of CS specimen). On the contrary, notch weakening was observed in the case of Al6061/Al₂O₃/20p. At 250°C both materials exhibited an increase of maximum net stress with stress concentration factor.

Fractographic analyses on specimens where final fracture was reached revealed that in all cases fracture occurred in a ductile manner, with the presence of relatively wide dimples. The presence, at the bottom of dimples, of reinforcement particles either cleaved or unbroken and displaying fragments of matrix or of reaction products on them is consistent with void formation and growth within the matrix following particle fracture or particle/interface debonding. Microstructural analyses performed on longitudinally sectioned broken specimens showed that at room temperature the microstructural damage mainly consisted in the cleavage of ceramic particles, often fractured by a single transversal crack. Independently on the notch geometry, cracks were roughly perpendicular to the loading direction and mainly involved coarser particles, as shown in Figure 3. Extensive damage occurred in conventional cylindrical tensile specimens (see maps in Figures 4a, 4b). Comparing these two maps it can be observed that the composite with the lowest reinforcement

volume of more homogeneous size reached relatively high fractions of fractured particles ($7\% < D_f < 10\%$). Slightly lower D_f values, of about 5%, can be seen in Al6061/Al₂O₃/20p, where fractures interested the largest particles.

In notched specimens the damage effects were less evident. Microstructural damage localized in regions closer to the specimen edge as the notch sharpness increased, as can be clearly seen in representative damage maps in Figure 5. Again, particle fracture was the main damage mechanism. This was the only form of microstructural damage observed when tension tests were interrupted at maximum load (examples in Figures 5c and 5d). In fractured notched specimens particle/matrix interface debonding was also observed, mainly occurring at particle edges perpendicular to the applied load and roughly localized in the same regions where other particle fractured.

In specimens tested at 250 °C (Figure 6) particle/matrix debonding prevailed (ratio D_d/D_f was greater than 1). The spatial distribution of this form of microstructural damage was substantially similar to that of particle fractured at room temperature. The relative importance of debonding decreased by increasing the volume fraction (and size) of particles, and increasing the notch sharpness of specimens.

NUMERICAL ANALYSIS OF THE STRESS FIELD

An elastoplastic finite element static analysis was performed for the NNP, 5N and 2N specimens, in order to define the evolution of the stress field within the notched area during the experimental tests, until the maximum applied load was reached. Axisymmetric models of half specimens gauge length were used for the numerical analysis. The materials were modelled as elastoplastic, homogenous and isotropic media. Distributed load at the modelled specimens ends was varied from zero to the maximum load of the corresponding experimental test.

The values of the maximum principal, equivalent, hydrostatic stress and of triaxiality (hydrostatic stress to Von Mises equivalent stress ratio) throughout the samples were calculated as function of the increasing applied load, without taking into account in the analyses the influence of the developing damage on the final stress field. Their representative maps of specimens 2N are here

reported in Figure 7. Specimens 2N at 20 and 250°C clearly show the influence of material and test temperature. It can be seen that hydrostatic and maximum principal stress localized in a region of minimum cross section. In Al6061/Al₂O₃/20p the peaks of maximum principal and hydrostatic stress were close to the specimen surface. In Al6061/Al₂O₃/10p, where highest maximum principal stress was reached, the region of high hydrostatic and maximum principal stress was less localized. At 250°C the hydrostatic and maximum principal stress maximum values and gradients within the specimens were significantly reduced (particularly in the Al6061/Al₂O₃/20p 5N specimen).

DISCUSSION

The ductile fracture of the investigated MMCs observed at both test temperatures originated by the presence of two main damage forms: fracture of alumina particles and matrix/interface debonding. The ratio between the percentage of debonded and fractured particles (D_d/D_f) was relatively variable with test temperature, macroscopic stress distribution and with the tested material.

Several papers [10, 16-17, 23] report particle fracture as the typical damage form for Al 6061 alloy reinforced by alumina particles. Such results were obtained by uniaxial tension tests at room temperature and perfectly correspond to the results of the present investigation on CS specimens, where D_f was relatively high and homogeneously distributed and particle cracked roughly perpendicularly to the applied load. Slightly higher D_f values were observed on Al6061/Al₂O₃/10p specimens, which displayed a greater strain to fracture. This fact could seem not in agreement with previous indirect measurements of microstructural damage by acoustic emission [15] and potential drop [24] techniques on the same materials, revealing that particle fracture occurred in the early stages of plastic deformation and that it accumulated with plastic strain more easily in the highly reinforced composite. Nevertheless, the higher propensity to fracture at low strain of the fraction of large ceramic reinforcement particles in Al6061/Al₂O₃/20p (explained in literature [16, 19, 25] as due to local constraint caused by different stiffness of matrix and particles) and the larger strain accumulated at fracture by Al6061/Al₂O₃/10p, having more homogeneous population of smaller alumina particles, can account for all these experimental results.

Even if particle fracture is not the only form of material damage, the observations on specimens from tests interrupted at maximum load indicated that it occurred before debonding become evident. Thus, an attempt to correlate D_f to the stress distribution under maximum load was done. It is worth to point out that the ‘macroscopic’ stress fields originated by the presence of notches were computed simply considering metal matrix composites as continuum media. The local stress fields acting on particles and matrix and directly responsible of the damage phenomena actually include also the effect of load redistribution and local constraint due to different stiffness of particle and matrix, depending on reinforcement volume fraction, size and shape and even on test temperature. The particle fracture was generally correlated to the magnitude of its tensile stress generated inside the particle in the load direction [4, 8, 19]. In any case, this stress can be indirectly modified by the presence of a multiaxial stress fields. Gonzales and Llorca [19] proposed a model where particle were assumed to fracture when they reached a critical value of maximum principal stress. Their model coupled with microstructural observations revealed that the application of external hydrostatic pressure was able to reduce and even to suppress particle fracture during concurrent tensile loading due to the reduction of the principal stress on particles at a given strain level of the matrix that allowed them to be strained up to higher values before cracking. On the other hand, in an experimental study Liu and Lewandowsky [17] observed that when a compressive hydrostatic stress was superimposed during tensile tests of on Al6061/Al₂O₃ particulate composite, it did not suppress particle fracture but only the void growth within the matrix from cracked particles. The effect of stress triaxiality on the microstructural damage of an Al6061/Al₂O₃/20p particulate composite was observed on fracture toughness specimens by Hadianfard et al. [16]. They suggested that in the region ahead the crack tip particle fracture was the dominant damage form of microstructural damage. At specimen surface, as the distance from the crack tip increased, particle fracture occurred in smaller amount and occurred in increasingly larger particles. At specimen mid thickness, the constraint reduced the number of fractured particles, that were also of smaller size. Crack bridging phenomena were observed only in this region of high constraint.

The notched specimens investigated in the present paper represent the case where a tensile triaxiality (here considered as the hydrostatic to Von Mises stress ratio) arose due to geometrical effects allowed the particles to sustain increased load to fracture with respect to the corresponding CS specimens. The comparison between damage and stress distribution maps at room temperature shows that as notch sharpness increased, the density of fractured particle decreased and localized in regions where both macroscopic maximum principal and hydrostatic stresses reached maximum values. In any case the definition of a correlation between particle fracture and the macroscopic applied state of stress is not straightforward, since the particle fracture distribution seems to be related both to maximum principal stress and to triaxiality, and peak values are in different regions. As a matter of fact the density of particle fractures appears to be affected by the presence of high triaxiality, which allows the composite to sustain locally higher critical maximum principal stress. The present investigation further revealed the presence of debonded particle-matrix interfaces. It is known that debonding is the predominant damage form when interfacial strength is relatively weak [1, 26]. Particle/matrix debonding in blocky shaped particles is generally located perpendicularly to the load axis. The stress field causing this form of microstructural damage was alternatively proposed to be the maximum principal stress (overloading a critical level dependent on the interface [1, 4]) or hydrostatic stresses localized in the matrix close to the particle edge [6]. All the factors locally increasing constraint (including ceramic particle size, shape) will reduce plastic flow and promote void nucleation and its following growth [6]. It was also reported in literature that in uniaxial tensile loading significant amount of cavitation occurred only after a certain plastic strain [4] and that voids extending gradually in the loading direction did not directly lead to fracture. In the presently investigated specimens, where early debonded particles were not distinguished in quantitative metallography analyses from voids extending from them, debonding was often located in the same regions where fractured particle were observed. It is reasonable that, after particle fracture in localized areas of the minimum cross section of specimen, the local stress increased and matrix further strained up to the early formation of debonding at unfractured particles.

Further results of the present investigation was the observation that on specimens tested at 250°C particle/matrix debonding prevailed over particle fracture when stress distribution tends to be uniform and that both D_f and D_d decreased in the notched specimens. Several factor can contribute to the lower damage sensitivity of the composite materials at high temperature. Of relative importance is the reduction of matrix strength and of its workhardening rate. Assuming that the mechanical behaviour of alumina particles is not modified when temperature is raised from 20 to 250°C, the above mentioned effects of temperature on the matrix cause local macroscopic and microscopic stress redistribution at relatively low applied load so that the critical maximum principal stress on particles causing their fracture is reached only in limited areas of notched specimens. On the contrary, void nucleation and growth in a matrix that at this temperature deforms plastically at low stress is relatively easy. This fact explains the greater (D_d/D_f) observed in the composites at the highest test temperature, and the limited localization of particle fracture in notched specimens. Previous studies [5,27] revealed a clear correlation between damage evolution and the achievable material strength. The delayed onset of material damage on the maximum net stress is also clearly visible in notched specimens, particularly at high temperature, where both forms of microstructural damage reduced and notch strengthening was observed in most cases.

CONCLUSIONS

Microstructural observations carried out on longitudinal sections of smooth and notched specimens pulled in tension confirmed the existence of two forms of material damage (particle fracture and matrix/particle debonding), the localization and relative importance of which were strictly dependent on the test temperature and on the stress field. At a given level of triaxiality particle fractured easily in regions of maximum principal tensile stress. The presence of fractured particles, even concentrated in specific regions of the minimum cross section of notched specimen increased the level of stress on the matrix that strained, depending on the triaxiality value, causing other particles to debond from the matrix. At high temperature the combination of matrix low strength

and of easier stress redistribution reduced the presence of particle fractures in favour of voids originated from matrix/particle debonding.

ACKNOWLEDGMENTS

The authors thank F. Luraschi and D. Barenghi for their technical support.

REFERENCES

- 1) T.W. Clyne, P. J. Withers. An introduction to metal matrix composites. Cambridge: University press, 1993.
- 2) D.J. Lloyd, Particle reinforced aluminium and magnesium matrix composites. *Int. Mater. Rev.* 1994; 39 (1); 1-23.
- 3) M. Li, S. Gosh, O. Richmond. An experimental-computational approach to the investigation of damage evolution in discontinuously reinforced aluminum matrix composite. *Acta Materialia* 1999; 47 (9); 3515-3532.
- 4) A.F. Whitehouse, T.W. Clyne. Cavity formation during tensile straining of particulate and short fibre metal matrix composite. *Acta Metall et Mat.* 1993; 41 (6); 1701-1711.
- 5) M. Vedani, E. Gariboldi. Damage and ductility of particulate and short fibre $Al-Al_2O_3$ composites, *Acta Mater.* 1996; 41 (8); 3077-3088.
- 6) J. Llorca, A. Needleman, S. Suresh. An analysis of the effects of metal void growth on deformation and ductility in metal-ceramic composites. *Acta Metall. Mater.* 1991; 39 (10); 2317-2335.
- 7) C. Gonzales, J. Llorca. An analysis of the effect of hydrostatic pressure on the tensile deformation of aluminum-matrix composites. *Mat. Sci. Eng.* 2002; A341; 256-263.
- 8) S. Ghosh, M. Li, S. Moorthy, K. Lee. Microstructural characterization, nano-scale modeling and multiple-scale analysis of discretely reinforced materials. *Mat. Sci. Eng.* 1998; A249; 62-70.

- 9) L.G. Lim, F.P.E. Dunne. Modeling void nucleation and growth processes in a particle-reinforced metal matrix composite material. *Computational Mater. Sci.* 1996; 5 (1-3); 177-186.
- 10) J.W. Luster, M. Thumann, R. Baumann. Mechanical properties of aluminium alloy 6061 Al_2O_3 . *Composites Mater. Sci, Techn.* 1993; 9 (10); 852 – 862
- 11) E. Gariboldi, M. Vedani. Creep damage of Al6061- Al_2O_3 particulate composite, *Int. J. Mat & Prod. Techn.* 2002; 17 (3/4); 243-260.
- 12) E. Gariboldi, M. Vedani. Creep and Creep Damage Tolerance of Al6061- Al_2O_3 Particulate Composites. *Adv. Eng. Mat.* 2002; 2 (11); 737-740.
- 13) G. Requena, H.P. Degischer, Effect of particle reinforcement on creep behaviour of AlSi1MgCu alloy. *Zeit. Metall.* 2005; 96 (7), 807-813.
- 14) Y.N. Rabotnov, Proc. 12th Int. Congress on Applied Mechanics, Stanford, 1968.
- 15) E. Gariboldi, C. Santullki, F. Stivali, M. Vedani. Valutazione del anneggiamento in materiali compositi a matrice metallica tramite monitoraggio di emissione acustica. XI IGF National Conference Proceedings, Brescia, Italy, 1995; p.235-243.
- 16) M.J. Hadianfard, J. Healy, Y.W. Mai. Fracture characteristics of a particulate-reinforced metal-matrix composite. *J. Mater. Sci.*, 1994, 29 (9), 2221-2227.
- 17) D.S. Liu, J.J. Lewandowsky. The effect of superimposed Hydrostatic pressure on deformation and fracture: Part II. Particulate Reinforced 6061 composites. *Met. Trans.* 1993; 25A; 699-615.
- 18) M.J. Hadianfard, G. Heness, J.C. Healy, Y-W. Mai. Fracture toughness measurements and failure mechanisms of metal-matrix composites. *Fatigue. Fract. Eng. Mater.* 1994; 17 (3); 253-263.
- 19) C. Gonzales, J. Llorca. An analysis of the effect of hydrostatic pressure on the tensile deformation of aluminum-matrix composites. *Mat. Sci. Eng.* 2002; A341; 256-263.

- 20) I.C. Stone, P. Tsakirooulos . The effect of reinforcement on the notched and unnotched room temperature tensile properties of Al-4wt%Cu/SiC_p MMCs. *Mat. Sci. Eng.* 1998; A241; 19-29.
- 21) M.F. Horstemeyer, K. Gall, K.W. Dolan, A. Waters, J.J. Haakins, D.E. Perkins, A.M. Gokhale, M.D. Dighe. Numerical, experimental, nondestructive and image analysis of damage progression in cast A356 aluminum notch tensile bars. *Theoret. and Appl. Fract. Mech.* 2003; 39(1); 23-45.
- 22) A.S. Argon, J. Im, A. Needleman. Distribution of plastic strain and negative pressure in necked steel and copper bars. *Metall. Trans.* 1975; 6A (4); 815-824.
- 23) N. Kanetake, M. Nomura, T. Choh. Continuous observation of microstructural degradation during tensile loading of particle reinforced aluminium matrix composites. *Mat. Sci. Technol.* 1995; 11 (12); 1246-1252.
- 24) E. Gariboldi, M. Vedani. Damage mechanisms in notched Al-based MMCs. *Advancing with Composites 2000 Conference Proceedings, Milan, Italy, 2000*; p. 251-257.
- 25) M. Mouzell, L. Weber, C. San Marchi, A. Mortensen. Influence of damage on the tensile behaviour of pure aluminium reinforced with =40vol. pct. alumina particles. *Acta Mater.* 2001; 49 (3), 369-379.
- 26) L.Z. Sun, J.W. Ju, H.T. Liu. Elastoplastic modeling of metal matrix composites with evolutionary particle debonding. *Mechanics of Materials* 2003; 35 (3-6); 559-569.
- 27) M. Vedani, F. D'Errico, E. Gariboldi. Mechanical and fracture behaviour of aluminum-based discontinuously reinforced composites at hot-working temperatures. *Comp. Sci. Tech* 2006; 66 (2); 343-349.

FIGURE CAPTIONS

Figure 1. Geometry of the specimens used for mechanical testing. From top to bottom: notched specimen with a root radius of 0,67 mm (5N), notched specimen with a root radius of 2,25 mm (2N), specimen with artificially machined neck profile (NNP), unnotched tensile specimen (CS).

Figure 2. Ratio between the maximum net stress to the UTS of the corresponding CS specimen as a function of the elastic stress concentration factor for different materials and test temperature.

Figure 3. Longitudinal sections of the specimens tested at room temperature: a) Al6061/Al₂O₃/10p, 2N specimen, 20°C, region of the notch root, b) Al6061/Al₂O₃/10p, 5N specimen, 20°C, region of the notch root. Extrusion direction and loading axis are vertical in micrographs.

Figure 4. Maps of D_f (on the left) and D_d (on the right) in the area of the final fracture in CS specimens: a) Al6061/Al₂O₃/20p, 20°C; b) Al6061/Al₂O₃/10p, 20°C, c) Al6061/Al₂O₃/10p, 250°C; d) Al6061/Al₂O₃/20p, 250°C. In figures 4 to 6 each rectangle corresponds to 450 X 320 μm^2 .

Figure 5. Maps of D_f (on the left) and D_d (on the right) in the region of the final fracture or of specimens tested at room temperature: a) Al6061/Al₂O₃/10p, 2N specimen; b) Al6061/Al₂O₃/10p, 5N specimen; c) Al6061/Al₂O₃/20p, 2N specimen; d) Al6061/Al₂O₃/20p, NNP specimen.

Figure 6. Maps of D_f (on the left) and D_d (on the right) in the region of the final fracture of specimens tested at 250°C: a) Al6061/Al₂O₃/10p, 2N specimen; b) Al6061/Al₂O₃/10p, 5N specimen; c) Al6061/Al₂O₃/20p, 2N specimen; d) Al6061/Al₂O₃/20p, 5N specimen.

Figure 7. Representative maps of hydrostatic stress (on the left), maximum principal stress (at centre) and triaxiality (on the right) within test specimens 2N (a-c) and 5N (d-e) under maximum applied load: a) Al6061/Al₂O₃/10p, 20°C; b) Al6061/Al₂O₃/20p, 20°C; c) Al6061/Al₂O₃/10p, 250°C; d) Al6061/Al₂O₃/10p, 20°C, e) Al6061/Al₂O₃/10p, 250°C. Values in iso-stress lines are in MPa..

Table I. Results of tensile tests on cylindrical specimens (CS) at 20 and 250°C

Material	Temperature (°C)	0.2%YS (MPa)	UTS (MPa)	A (%)	n	K (MPa)
10% Al ₂ O ₃	20	312	359	8.6	0.055	439.
20% Al ₂ O ₃	20	331	368	5.1	0.044	442
10% Al ₂ O ₃	250	171	179	12.4	0.030	207
20% Al ₂ O ₃	250	167	189	7.5	0.059	246

ACCEPTED MANUSCRIPT

Fig 1:



Fig 2:

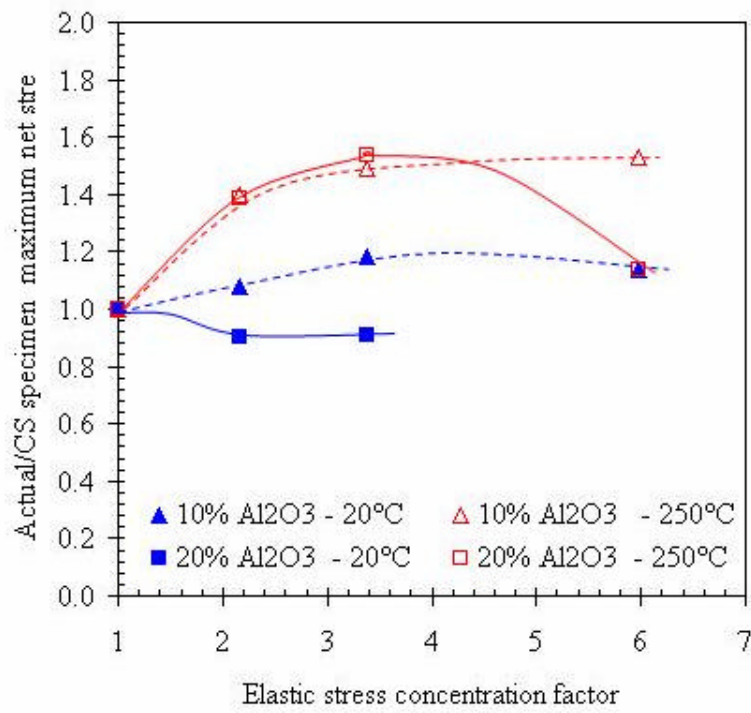


Fig 3:

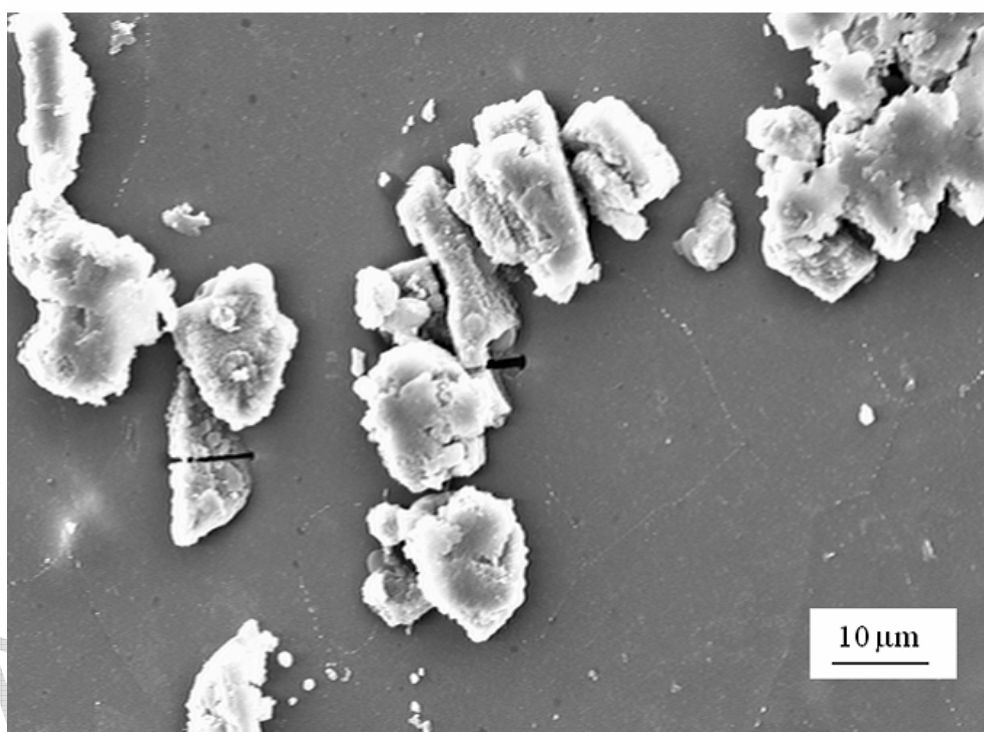
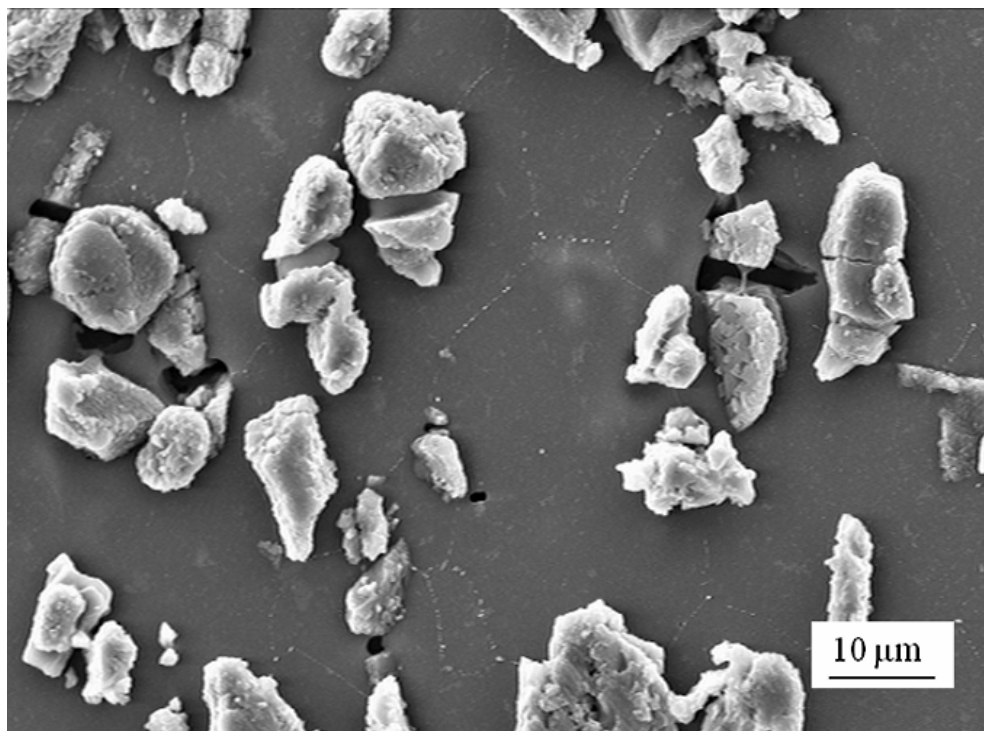
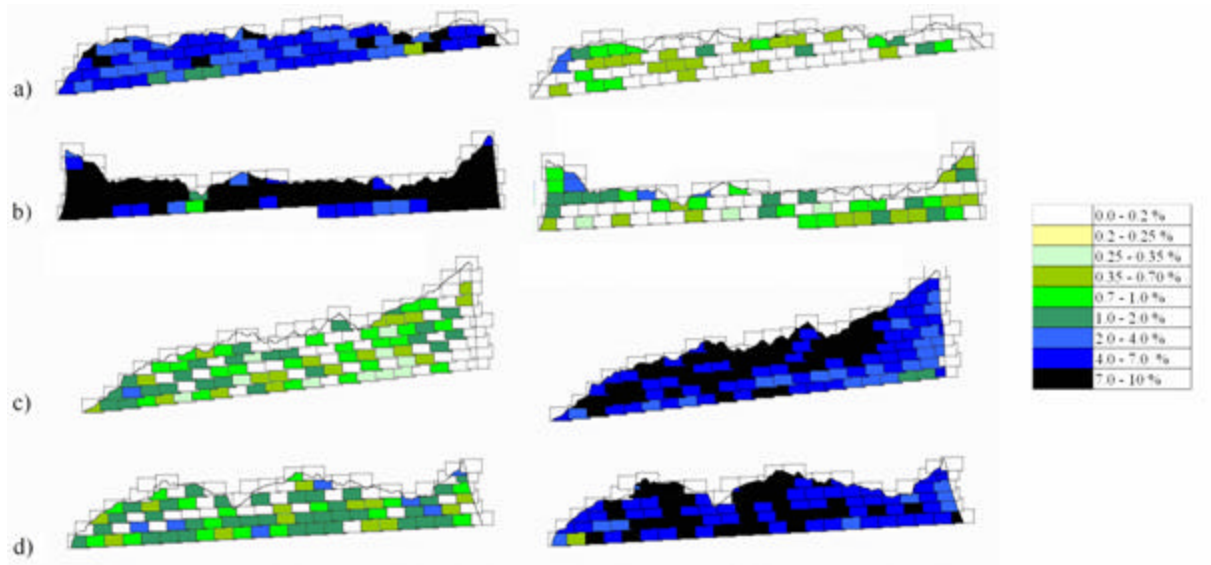
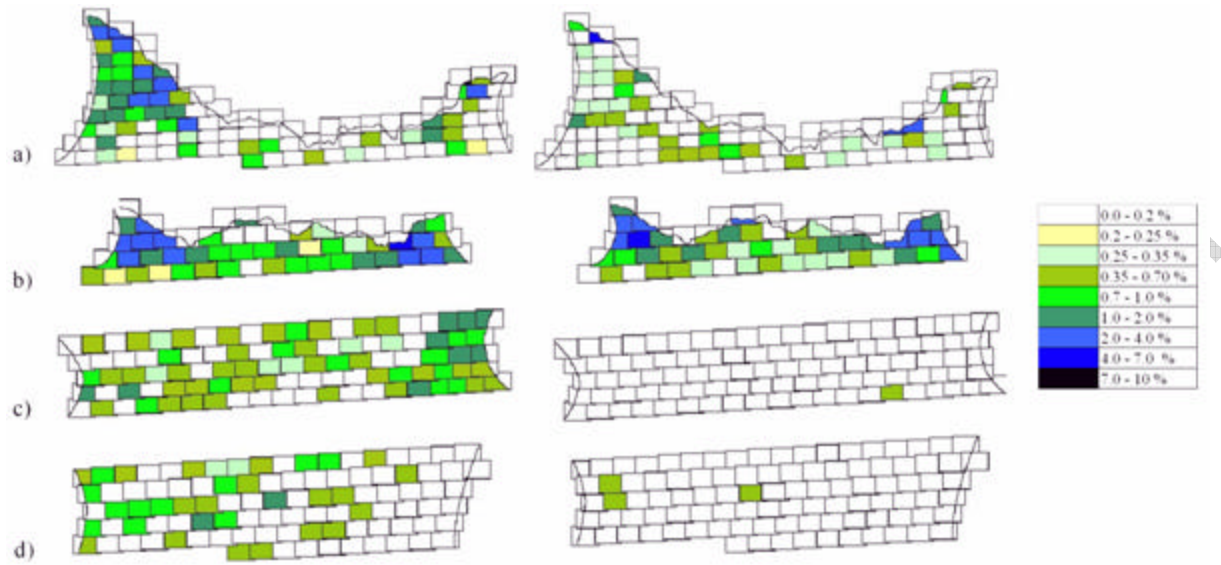


Fig 4:



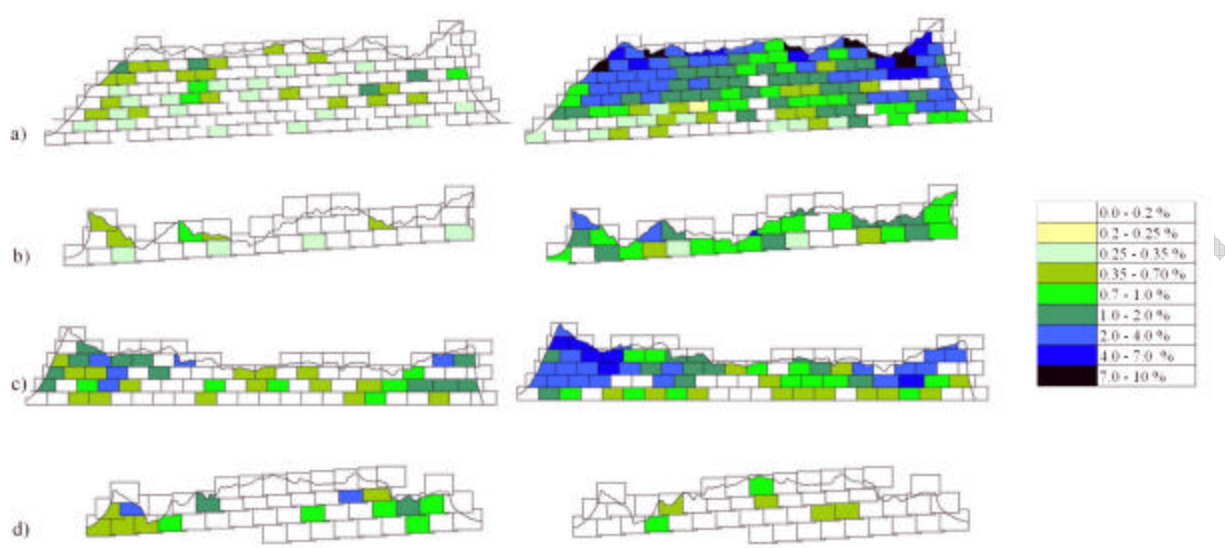
ACCEPTED MANUSCRIPT

Fig 5:



ACCEPTED MANUSCRIPT

Fig 6:



ACCEPTED MANUSCRIPT

Fig 7:

